Journal of the Optical Society of Korea, Vol. 7, No. 1, March 2003, pp. 7-12

Band Structure Analysis of Strained Quantum Wire Arrays

Jong Chang Yi* and Jeong-Beom Ji

School of Electronic and Electrical Engineering, Hong Ik University, Seoul 121-791, KOREA

(Received November 14, 2002)

A numerical approach for the analysis of quantum wire structures has been presented using a finite-element method which includes the strain analysis and the band analysis of the Luttinger-Kohn Hamiltonian with the deformation potential. A systematic implementation of the multiband Hamiltonian in the finite-element scheme is outlined and the corresponding variational functional is derived for arbitrarily shaped strained quantum wire arrays. This method is then applied to calculate the band structures of strained quantum wire arrays.

OCIS codes : 160.6000, 230.5590, 140.5960.

I. INTRODUCTION

Strained quantum wire structures, which provide an additional quantum confinement due to the deformation potential, have undergone extensive study and development for their enhanced optical gain compared to the unstrained counterpart [1–4]. Obviously the main purpose of fabricating quantum wires is to generate semiconductor heterostructures with properties superior to quantum wells. The lateral superlattice is one of the most promising structures for its small size and higher wire density [5–7]. One drawback, however, is the relatively weak lateral confinement due to the lateral material intermixing [6,7]. Recent successes in the fabrication of the strained lateral superlattice quantum wire structures point to the possibility of additional lateral confinement due to the deformation potential [1,2]. In this paper, a systematic methodology will be presented to analyze the band structures of quantum wire arrays to assess the effect of the strain on the optical properties of the quantum wire structures.

II. LUTTINGER-KOHN HAMILTONIAN FOR STRAINED SEMICONDUCTORS

Strain in a crystal causes deformation in the atomic geometry which in turn results in a new crystalline potential. If the strain is weak enough to preserve the lattice periodicity, the effect of the strain in the periodic structure can be analyzed by perturbation theory as [8,9]

$$\mathbf{H_1} = \begin{bmatrix} \mathbf{D_{st}} & 0 \\ 0 & \mathbf{D_{st}} \end{bmatrix} + \mathbf{H_0} \tag{1}$$

where

$$\mathbf{D_{st}} = \begin{bmatrix} l\epsilon_{xx} + m(\epsilon_{yy} + \epsilon_{zz}) & n\epsilon_{xy} & n\epsilon_{xz} \\ n\epsilon_{yx} & l\epsilon_{yy} + m(\epsilon_{xx} + \epsilon_{zz}) & n\epsilon_{yz} \\ n\epsilon_{zx} & n\epsilon_{zy} & l\epsilon_{zz} + m(\epsilon_{xx} + \epsilon_{yy}) \end{bmatrix} \tag{2}$$

is the orbital strain Hamiltonian for $6p$ orbitals, and $\mathbf{H_0}$ is the unperturbed Hamiltonian [10–12]. l, m, and n are the strain matrix elements and $\epsilon_{\alpha\beta}$'s are the strain tensor with α and β running through x, y, and z. Eq. (1) has a great similarity to the $\mathbf{k}\cdot\mathbf{p}$ Hamiltonian. As a result, the 4 band orbital strain Hamiltonian for HH and LH bands would have the same form as the Luttinger-Kohn Hamiltonian under unitary transformation and crystal rotation [13,14]. It can be directly obtained from the $\mathbf{k}\cdot\mathbf{p}$ Hamiltonian [10] by substituting A , B , C, and $k_\alpha k_\beta$ with l, m, n and $\epsilon_{\alpha\beta}$, respectively. Conventionally the strain ma-

trix elements are expressed in terms of the deformation potential constants as [13,15]

$$a_\nu = \frac{l+2m}{3} \qquad b = -\frac{l-m}{3} \qquad d = -\frac{n}{\sqrt{3}} \quad (3)$$

where a_ν represents the valence band energy change due to the hydrostatic stress, and b and d represent the splitting of the HH and LH bands due to the uniaxial stress along [001] and [111] directions, respectively [16]. The sign convention is taken positive for the energy lower than the top of the bulk valence band. The expressions in (3) also have similar forms with the Luttinger parameters in the $\mathbf{k}\cdot\mathbf{p}$ Hamiltonian [10]. By comparing these two equations, one can find the coefficients of the 4 band strain Hamiltonian from the unperturbed Hamiltonian [11] by substituting [14]

$$\gamma_1 \rightarrow a_\nu \qquad \gamma_2 \rightarrow -\frac{b}{2} \qquad \gamma_3 \rightarrow -\frac{d}{2\sqrt{3}} \quad (4)$$

For instance, the 4 band strain Hamiltonian for cubic axes orientation can be expressed as

$$\mathbf{H_{st}} = \begin{bmatrix} p+q & r & s & 0 \\ r^\dagger & p-q & 0 & s \\ s^\dagger & 0 & p-q & -r \\ 0 & s^\dagger & -r^\dagger & p+q \end{bmatrix} \quad (5)$$

where

$$\begin{aligned} p &= a_\nu(\epsilon_{xx}+\epsilon_{yy}+\epsilon_{zz}) \\ q &= -\frac{b}{2}(\epsilon_{xx}+\epsilon_{yy}-2\epsilon_{zz}) \\ r &= d(\epsilon_{yz}+i\epsilon_{zx}) \\ s &= -\frac{\sqrt{3}}{2}b(\epsilon_{xx}-\epsilon_{yy})+id\epsilon_{xy} \end{aligned} \quad (6)$$

When the crystal orientation is 45° rotated in $(x-y)$ plane, s modifies to

$$s = -\frac{1}{2}d(\epsilon_{xx}-\epsilon_{yy}) + i\sqrt{3}b\epsilon_{xy}. \quad (7)$$

The expressions in (6) and (7) are slightly different from the expressions commonly referred in the literatures [17,18]. This is because the phase of the unitary matrix for the 6 band spin orbit Hamiltonian is taken directly from the Luttinger-Kohn formulation [10] while others take it alternatively [19]. Variations in the definition of the deformation potential also diversified the coefficients of the strain Hamiltonian. A detailed comparison can be found in the Kane's work [20] for the various stress orientations in the crystal.

Using the strain Hamiltonian in (5), the top of the valence band structure can be analyzed by finding the solution of the variational functional

$$\begin{aligned} J = &< \mathbf{J}_\nu|\mathbf{H_{LK}}+\mathbf{H_{st}}+V(y,z)\mathbf{I}|\mathbf{J}_\nu > \\ &- < J_\nu|E|J_\nu >= 0 \end{aligned} \quad (8)$$

using the finite-element method as discussed in the previous section.

Like the $\mathbf{k}\cdot\mathbf{p}$ Hamiltonian, the strain affects the conduction band energy levels too. Since the conduction band has a spherically symmetric basis function, only the diagonal components of the strain tensor have non-zero perturbation. Thus the energy level shift in the conduction band can be expressed as

$$\Delta E_c = a_c(\epsilon_{xx}+\epsilon_{yy}+\epsilon_{zz}) \quad (9)$$

where a_c is the deformation potential in the conduction band due to the hydrostatic stress. Here $\epsilon_{xx}+\epsilon_{yy}+\epsilon_{zz}$ represents the ratio of the volume change, $\Delta V/V$.

One thing to note in the valence band is that both the HH and LH valence bands shift by $p = a_\nu(\epsilon_{xx}+\epsilon_{yy}+\epsilon_{zz})$. Thus the bandgap change due to the strain effect can be expressed as

$$\Delta E_g = (a_c+a_\nu)(\epsilon_{xx}+\epsilon_{yy}+\epsilon_{zz}) \quad (10)$$

For uniaxial stress along [001] direction, the strain coefficient can be expressed as [21]

$$\begin{aligned} \epsilon_{xx} = \epsilon_{yy} &= \frac{a_{sub}-a_{layer}}{a_{layer}} \\ \epsilon_{zz} &= -2\frac{C_{12}}{C_{11}}\epsilon_{xx} \end{aligned} \quad (11)$$

where a_{sub} and a_{layer} denote the lattice constants of the substrate and the strained layer, respectively. C_{11} and C_{12} are the elastic constants. Then the volume change $\epsilon_{xx}+\epsilon_{yy}+\epsilon_{zz}$ can be expressed in terms of ϵ_{xx}, hence the band gap change can be simplified to [21]

$$\Delta E_g = a\frac{2(C_{11}-C_{12})}{C_{11}}\epsilon_{xx} \quad (12)$$

where $a = a_c + a_\nu$. The sign of the deformation potential is negative in most III-V semiconductors and C_{11} is always larger than C_{12}. Therefore, the bandgap change has the opposite sign to the strain coefficient. With the compressive strain, where the lattice constant of the layer is larger than that of the substrate, the energy gap increases by ΔE_g since a and ϵ_{xx} in (12) are both negative. Thus the conduction band shifts upwards by a_c/a of the total bandgap change and the valence band shifts downwards by a_ν/a of the bandgap change as shown in Fig. 1. The opposite will happen for the tensile strain [22].

The splitting of the HH and LH bands can be estimated from the eigenvalues of the strain Hamiltonian in (5). The 4×4 matrix has two twofold degenerate

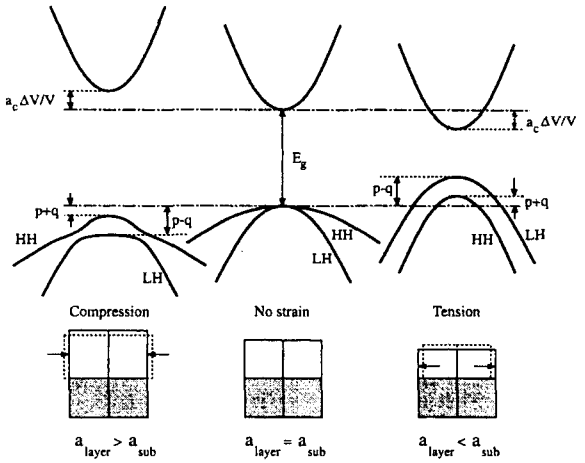

FIG. 1. Band diagrams of a strained semiconductor bulk under the uniaxial strain along [001] direction [22].

eigenvalues at the zone center [18] as

$$\Delta E_{HH} = p + sgn(q)\sqrt{q^2 + |r|^2 + |s|^2}$$
$$\Delta E_{LH} = p - sgn(q)\sqrt{q^2 + |r|^2 + |s|^2} \qquad (13)$$

each one for the HH and LH subband, respectively. Here the effect of the SO band is neglected. For the uniaxial strain along the [001] direction, r and s becomes zero from (11) and (6) since the shear strain is zero and $\epsilon_{xx} = \epsilon_{yy}$. Then the energy gap between the LH band to HH band becomes [21,22]

$$\Delta(E_{LH} - E_{HH}) = -2q = b\frac{C_{11} + 2C_{12}}{C_{11}}\epsilon_{xx} \qquad (14)$$

Since the uniaxial deformation potential, b, is negative in most III-V semiconductors [16], the splitting between the LH and HH bands has the opposite sign with the strain coefficient. In other words, with the compressive strain, the HH subbands have smaller energies with respect to the valence band top, hence they shift towards the top of the valence band. The LH subbands shift toward lower valence band energy. With the tensile strain, the LH subbands have smaller energies than HH subbands hence they shift to above the HH subbands as shown in Fig. 1.

III. STRAIN PROFILE IN QUANTUM WIRE ARRAY

In quantum wires the strain profile is no longer uniaxial when the lattice constant along the lateral direction is not uniform. The lattice constants of the quantum wire layer, the barrier layer, and the substrate can be all different. In that case there exists the shear stress as well as the hydrostatic stress. Thus those strain coefficients need to be calculated first for a realistic strain Hamiltonian analysis. There are several numerical techniques to calculate the strain profile including the finite-difference method and the finite-element methods [23,24]. In this paper the strain profile will be calculated using the linearized finite-element technique [11]. If the stress in the material is sufficiently below the nonlinear regime or the rupture condition, the strain is linearly proportional to the stress governed by the Hook's law [25]. Then the elastic strain energy can be expressed in terms of the linear strain coefficients as [26,27]

$$U = \int_V dV \left[\frac{1}{2}C_{11}(\epsilon_{xx}^2 + \epsilon_{yy}^2 + \epsilon_{zz}^2) + 2C_{44}(\epsilon_{xy}^2 + \epsilon_{yz}^2 + \epsilon_{zx}^2) + C_{12}(\epsilon_{yy}\epsilon_{zz} + \epsilon_{zz}\epsilon_{xx} + \epsilon_{xx}\epsilon_{yy})\right]. \qquad (15)$$

Using the linearized Galerkin method, the strain coefficients can be expressed in terms of the lattice coordinates [25]. Fig. 2 shows the lattice deformation due to the strain in the crystal. The coordinate of the each intersection of the lattice grid is given by (u, ν, w) and the coordinates of the computing grid are given by (x, y, z). Since the quantum wires are uniform along the x-axis, only the νw and yz plane are shown. If one assumes that the crystal is strained to match the substrate lattice constant along the wire direction, the x components of the strain tensor can be expressed as

$$\epsilon_{xx} = \frac{a_{sub} - a_i}{a_i}$$
$$\epsilon_{xy} = \epsilon_{xz} = 0 \qquad (16)$$

where a_i is the lattice constant of the unstrained

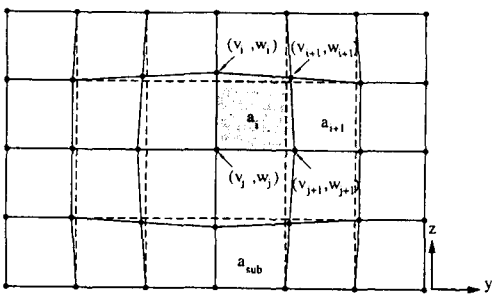

FIG. 2. Cross section of the strained lattice profile. The regular dashed grid is the computing window (y, z) and the deformed solid grid represents the actual lattice geometry (ν, w). The x and u coordinates are omitted since they are uniform along the direction into the figure. a_i is the lattice constant of the unstrained material in the i-th rectangle, and a_{sub} is that of the substrate.

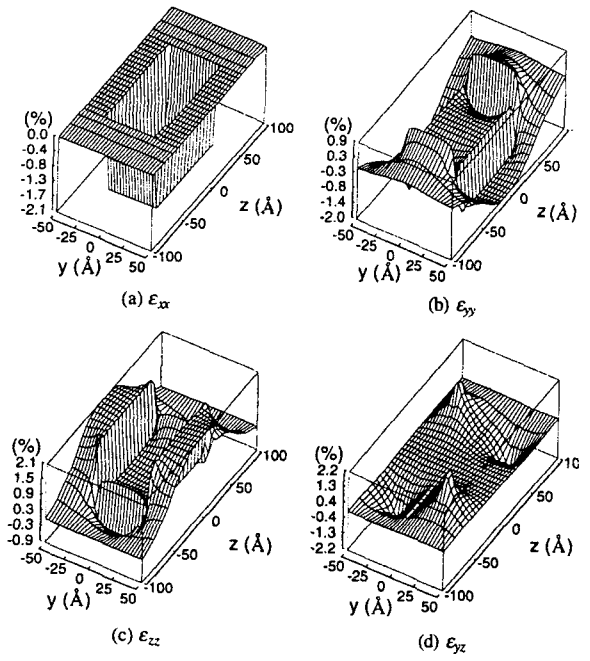

FIG. 3. Profiles of the strain tensor in a 50 Å wide 100 Å thick $In_{0.3}Ga_{0.7}As$ quantum wire array surrounded by $Al_{0.4}Ga_{0.6}As$. (a) ϵ_{xx}, (b) ϵ_{yy}, (c) ϵ_{zz}, and (d) ϵ_{yz}. The quantum wires are parallel to the x-axis and are distributed along the y-axis.

material in the i-th rectangle, and a_{sub} is the lattice constant of the substrate as shown in Fig. 2.

The strain coefficients along the transverse direction can be expressed in terms of the lattice coordinates as mentioned earlier. For the i-th rectangle, one can estimate the strain coefficients as

$$\begin{aligned}
\epsilon_{yy} &= \frac{1}{2}\left(\frac{\nu_{i+1}-\nu_i}{y_{i+1}-y_i}+\frac{\nu_{j+1}-\nu_j}{y_{j+1}-y_j}\right)-\frac{a_i}{a_{sub}} \\
\epsilon_{zz} &= \frac{1}{2}\left(\frac{w_{i+1}-w_{j+1}}{z_{i+1}-z_{j+1}}+\frac{w_i-w_j}{z_i-z_j}\right)-\frac{a_i}{a_{sub}} \\
\epsilon_{yz} &= \frac{1}{2}\left(\frac{\partial w}{\partial y}+\frac{\partial \nu}{\partial z}\right)
\end{aligned} \tag{17}$$

where

$$\begin{aligned}
\frac{\partial w}{\partial y} &= \frac{1}{2}\left(\frac{w_{i+1}-w_i}{y_{i+1}-y_i}+\frac{w_{j+1}-w_j}{y_{j+1}-y_j}\right) \\
&\quad -\frac{1}{2}\left(\frac{z_{i+1}-z_i}{y_{i+1}-y_i}+\frac{z_{j+1}-z_j}{y_{j+1}-y_j}\right) \\
\frac{\partial \nu}{\partial z} &= \frac{1}{2}\left(\frac{\nu_{i+1}-\nu_{j+1}}{z_{i+1}-z_{j+1}}+\frac{\nu_i-\nu_j}{z_i-z_j}\right) \\
&\quad -\frac{1}{2}\left(\frac{y_{i+1}-y_{j+1}}{z_{i+1}-z_{j+1}}+\frac{y_i-y_j}{z_i-z_j}\right).
\end{aligned} \tag{18}$$

The (y_i, z_i) is the coordinate of the crossing point of the dashed grid corresponding to (ν_i, w_i), and so on so forth. Substituting the strain coefficients in (15) using (16)–(18) one can express the elastic internal energy U in terms of the deformed lattice coordinates (ν, w). The variation principle states that the internal energy becomes minimum at the correct strain profile. Thus the strain profile can be obtained by minimizing U with respect to the lattice coordinates, $\mathbf{S} = (\cdots \nu_i, w_i, \nu_{i+1}, w_{i+1}, \cdots)^T$, as

$$\frac{\partial U}{\partial \mathbf{S}} = \mathbf{K_s S} + \mathbf{M_s} = \mathbf{0} \tag{19}$$

where $\mathbf{K_s}$ and $\mathbf{M_s}$ are the matrices resulting from (15). Eq. (19) leads to a boundary value problems [21] for the lattice coordinates, $\mathbf{S}$. This can be solved using the standard linear algebra procedures such as the LU decomposition or SOR algorithm [26,27]. From the lattice coordinates, one can obtain the values of the strain coefficients using (16)–(18) again.

Fig. 3 shows the cross-sectional profiles of the non zero components of the strain tensor in a 50 Å wide 100 Å thick $In_{0.3}Ga_{0.7}As$ quantum wire array surrounded by $Al_{0.4}Ga_{0.6}As$. The InGaAs and AlGaAs material parameters are listed in the reference [16].

IV. RESULTS

The band discontinuities in the conduction and the valence band without the strain effect are 663 meV and 285 meV, respectively. The lattice constants of the wire material and the surrounding material are 5.7748 Å and 5.6574 Å, respectively, yielding 2.1 % lattice mismatch between them. The strain profile of ϵ_{xx} is uniform inside the quantum wire and has a negative value since the wire material has a larger lattice constant that the substrate as expressed in (16). The strain profiles for ϵ_{yy} and ϵ_{zz} are strongly distorted due to the lattice mismatch along the vertical and horizontal directions. The shear strain ϵ_{yz} shows a point symmetric profile with peak values at the corners of the quantum wire rectangle. One thing to note here

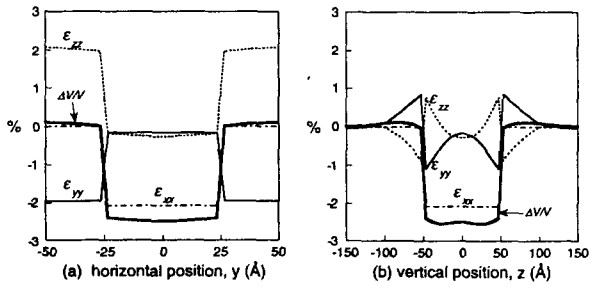

FIG. 4. The horizontal strain profile along the y-axis at $z = 0$ (a), and the vertical strain profile along the z-axis at $y = 0$ (b). Thick lines indicate the volume change $\Delta V/V = \epsilon_{xx} + \epsilon_{yy} + \epsilon_{zz}$.

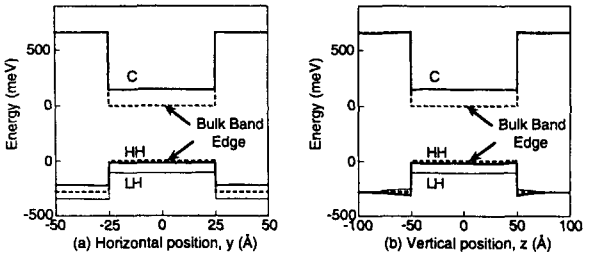

FIG. 5. The horizontal band profile along the y-axis at $z = 0$ (a), and the vertical band profile along the z-axis at $y = 0$ (b). The dashed lines indicate the bulk band positions for the unstrained materials.

is that the ϵ_{yy} and ϵ_{zz} have the opposite values, i.e., their signs are opposite and the magnitudes are almost the same. Thus the summation of ϵ_{xx} , ϵ_{yy}, and ϵ_{zz} is almost the same with ϵ_{xx} since ϵ_{yy} and ϵ_{zz} canceled each other out. Fig. 4 shows the strain profile along the lateral direction and along the vertical direction at the center of the quantum wire. Unlike the uniaxial stress as in the quantum well structures, the quantum wire structure has non uniform ϵ_{yy} and ϵ_{zz} profiles as shown in Fig. 4. Thus, the HH and LH band separation cannot be simplified to the expression in (14) where the energy separation is proportional to ϵ_{xx}.

The band profiles of the conduction band, heavy hole and light hole bands are instead estimated using (9) and (13), and are plotted in Fig. 5. If there is no strain effect, the conduction and the valence band offsets are 663 meV and 285 meV, respectively. Due to the compressive strain inside the quantum wires, the conduction band in the quantum wires shifts upward and the valence bands shift downward. However, in the compressive strain, the signs of p and q in (16) are opposite with each other, and the magnitudes of the deformation potentials p and $\sqrt{q^2 + |r|^2 + |s|^2}$ are almost the same. Hence the shift of the HH band is actually quite small, while the LH band is suppressed down simultaneously by the hydrostatic strain term p and the uniaxial strain term $\sqrt{q^2 + |r|^2 + |s|^2}$. Quantitatively, the conduction band moves upwards by 148 meV, and the HH band moves downwards by 21 meV, whereas the LH band moves downwards by 107 meV at the center of the quantum wires, yielding 86 meV of the HH-to-LH band separation. Hence the conduction band and the heavy hole band offsets along the lateral direction are modified to 514 meV and 201 meV, respectively.

The eigen energy levels in this strained quantum wire array and its optical properties will be discussed in the next subsection including the comparisons to various types of strained quantum wire arrays and the unstrained quantum wire arrays

V. CONCLUSIONS

In this paper an efficient finite-element method has been developed to numerically solve the Luttinger-Kohn Hamiltonian for the strained quantum wire arrays. The required variational functional is formulated through integration by parts with proper boundary conditions. This method offers a significant computational advantage compared to other methods and can be applied to any arbitrarily shaped geometry. The strain profile is rigorously calculated numerically including the hydrostatic and the shear strain components using the linearized Galerkin method. The effect of the strain in the various types of the strained quantum wire arrays are quantitatively analyzed for the InGaAs quantum wire arrays. This method will provide a very efficient numerical tool for the analysis of the polarization dependence of the optical gain in the actual quantum wire arrays.

*Corresponding author : wave@hongik.ac.kr.

REFERENCES

[1] K. Y. Cheng, E. M. Stellini, P. J. Pearah, A. C. Chen, A. M. Moy, and K. C. Hsieh, International Electron Device Meeting '92(IEEE), 875 (1992).

[2] P. J. Pearah, E. M. Stellini, A. C. Chen, A. M. Moy, K. C. Hsieh, and K. Y. Cheng, Appl. Phys. Lett. **62**, 729 (1993).

[3] M. Walther, E. Kapon, C. Caneau, D. M. Hwang, and L. M. Schiavone, Appl. Phys. Lett. **62**, 2170 (1993).

[4] T. Yamauchi, T. Takahashi, and Y. Arakawa, Surface Science **267**, 291 (1992).

[5] J. C. Yi, N. Dagli, and L. A. Coldren, Appl. Phys. Lett. **59**, 3015 (1991).

[6] M. S. Miller, H. Weman, C. E. Pryor, M. Krishnamurthy, P. M. Petroff, H. Kroemer, and J. L. Merz, Phys. Rev. Lett. **68**, 3464 (1992).

[7] R. C. Miller, D. A. Kleinman, and A. C. Gossard, Phys. Rev. B **29**, 7085 (1984).

[8] G. E. Pikus and G. L. Bir, Sov. Phys.-Solid State **1**, 1502 (1960).

[9] G. E. Pikus and G. L. Bir, *Symmetry and strain-induced effects in semiconductors*, (Wiley, New York ,1974) Chapter 3.

[10] J. M. Luttinger and W. Kohn, Phys. Rev. **97**, 869 (1955).

[11] J. C. Yi and N. Dagli, IEEE J. Quantum Electron. **31**, 208 (1995).

[12] I. Suemune and L. A. Colderen, IEEE J. Quantum Electron. **24**, 1778 (1988).

[13] S. L. Chuang, *Physics of Optoelectronic Devices*, (Wiley Inter Science, New York, USA, 1995) Chapter 4.

[14] D. Ahn and S. L. Chuang, IEEE J. Quantum Electron. **24**, 2400 (1988).

[15] T. P. Bahder, Phys. Rev. B **41**, 11992 (1990).
[16] Landolt-Bornstein, *Numerical Data and Functional Relationships in Science and Technology*, (Springer, Berlin, 1982), vols. 17 and 22a.
[17] I-H. Tan, M. Y. He, J. C. Yi, E. Hu, N. Dagli, and A. Evans, J. Appl. Phys. **72**, 546 (1992).
[18] C. Y. P. Chao and S. L. Chuang, Phys. Rev. B **46**, 4110 (1992).
[19] S. W. Corzine, private communications.
[20] E. O. Kane, Phys. Rev. **178**, 1368 (1965).
[21] G. Ji, D. Huang, U. K. Reddy, T. S. Henderson, R. Houdre, and H. Morkoc, J. Appl. Phys. **62**, 3366 (1987).
[22] S. L. Chuang and C. Y. P. Chao, Phys. Rev. B **43**, 9649 (1991).
[23] O. C. Zienkiewicz, *Developments in stress analysis*, (Applied Science Pub. Ltd., London, 1979) Chapter 1.
[24] Z. Xu and P. M. Petroff, J. Appl. Phys. **69**, 6564 (1991).
[25] S. F. Borg, *Fundamentals of engineering elasticity*, (D. Van Nostrand Co. Ltd., New York, 1962) Chapters 3-4.
[26] K.-J. Bathe and E. L. Wilson, *Numerical Methods in Finite Element Analysis*, (Prentice-Hall, Inc., Englewood Cliffs, New Jersey 1976) Chapter 6.
[27] P. P. Silvester and R. L. Ferrari, *Finite Elements For Electrical Engineers*, (Cambridge University Press, London 1983) Chapter 1.